Nanoscale

RSC Publishing

PAPER

View Article Online
View Journal | View Issue

Cite this: *Nanoscale*, 2013, **5**, 7397

Self-supported Pt nanoclusters *via* galvanic replacement from Cu_2O nanocubes as efficient electrocatalysts†

Qing Li,[ac] Ping Xu,*[ab] Bin Zhang,[a] Gang Wu,[c] Hongtao Zhao,[a] Engang Fu[c] and Hsing-Lin Wang*[b]

Received 2nd May 2013
Accepted 4th June 2013

DOI: 10.1039/c3nr02243a

www.rsc.org/nanoscale

A novel synthesis method for self-supported Pt nanoclusters (Pt NCs) comprised of interconnected 2–3 nm Pt nanoparticles was developed by employing the galvanic replacement process between Cu_2O nanocubes and $PtCl_4^{2-}$ ions. This discovered synthesis procedure eliminates the use of any polymer capping agents and enables a catalytically clean Pt surface. It is determined that the presence of H^+ ions is crucial for initializing the galvanic replacement reaction. The electrocatalytic performances of the Pt NCs were tested for both oxygen reduction and methanol oxidation reactions, which showed higher electrochemical activity and greater long-term durability as compared with commercial Pt materials.

Introduction

Platinum (Pt)-based nanostructures have attracted considerable interest owing to their various potential applications derived from their unique catalytic, electronic, and sensing properties.[1,2] Particularly, Pt remains the most effective catalyst to facilitate both hydrogen oxidation and oxygen reduction in fuel cells.[3] Current Pt electrocatalysts primarily consist of Pt nanoparticles (NPs) supported on carbon blacks (Pt/C). However, a fast and significant loss of electrochemically active surface area (ECSA) and thus degradation of fuel cell efficiency is often observed with the Pt/C catalysts over time. Such phenomena can be mainly ascribed to the corrosion of carbon supports, Ostwald ripening and agglomeration of Pt NPs, and thus loss of collective electrocatalytic sites.[4,5] Another mechanism associated with ECSA loss is that the Pt surface tends to be covered by oxygen-containing species (*e.g.* hydroxyl groups) during continuous fuel cell operation.[6] To overcome these challenges, Pt nanostructures with controlled morphology and size are extensively explored to mitigate the drawbacks of carbon and minimize the possible Pt oxidation.

The catalytic activity of Pt nanomaterials depends strongly on their size, shape, composition, crystallinity, and surface structures. Thus, various approaches have been developed to control the size and shape of Pt nanostructures through physical, chemical, and even biological methods so as to maximize their electrocatalytic properties.[7] Among them, solution chemistry processes appear more appropriate to synthesize Pt NPs of well-defined size and shape with a lower price tag.[8] Until now, a variety of Pt nanostructures, including polyhedra,[2,9–11] wires,[12–14] tubes,[15,16] and dendrites,[17,18] have been synthesized by manipulating growth at specific crystal surfaces or templated (seeded) methods, where capping agents or polymer surfactants are typically introduced to stabilize high-energy surfaces of the Pt nanocrystals. However, electrocatalytic reactions such as the oxygen reduction reaction (ORR) and methanol oxidation reaction (MOR) occur effectively on catalytically "clean" NPs as the reactants effectively adsorb onto active sites free of stabilizing agents.[1] If the interaction between the stabilizing agent and metal surface is too strong, the catalytic activity will be greatly reduced. Removal of organic ligands (surfactants) from colloidal Pt NPs has been shown to enhance their catalytic performances,[19] revealing a strong correlation between the catalytic activity of Pt nanomaterials and surface properties. Very recently, Lee *et al.*[20] reported an electroless Pt deposition on Mn_3O_4 NPs *via* a galvanic replacement process occurring between Mn_3O_4 and $PtCl_4^{2-}$ complexes, and the obtained Pt/Mn_3O_4 showed enhanced electrocatalytic performance for the ORR. Liu *et al.*[21] also reported an *in situ* growth of Au NPs on the surfaces of Cu_2O nanocubes, which involves the reduction of Au^{3+} ions by Cu_2O. Preparation of noble metal NPs through the reduction of metal ions by metal oxide with an intermediate oxidation state renders a clean surface of the as-prepared metal NPs, which might become a facile and novel method in metal NP synthesis for various applications.

As for the applications in fuel cells, Pt or its alloy nanoclusters (NCs) that are formed by assembly of NPs with sizes <10 nm typically showed superior catalytic activities, resulting from the size and structure effects.[1–3] Meanwhile, porous Pt nanostructures could be better electrocatalysts for energy

[a]*Department of Chemistry, Harbin Institute of Technology, Harbin 150001, China. E-mail: pxu@hit.edu.cn; Fax: +86-451-86418750; Tel: +86-451-86413702*

[b]*Chemistry Division, Los Alamos National Laboratory, Los Alamos, NM 87545, USA. E-mail: hwang@lanl.gov; Tel: +1-505-665-6811*

[c]*Materials Physics and Applications Division, Los Alamos National Laboratory, Los Alamos, NM 87545, USA*

† Electronic supplementary information (ESI) available: Fig. S1–S9. See DOI: 10.1039/c3nr02243a

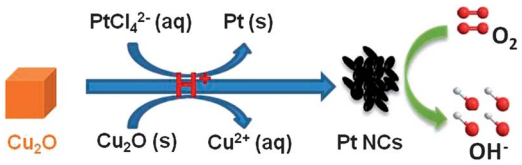

Scheme 1 Synthesis of self-supported Pt nanoclusters (NCs) *via* a galvanic replacement method from Cu_2O nanocubes for the oxygen reduction reaction. The "H^+" is highlighted in red to show that without supplying H^+ ions, this reaction would not proceed.

devices than other Pt structures.[22,23] Herein, we demonstrate for the first time the synthesis of self-supported Pt NCs consisting of 2–3 nm NPs *via* a galvanic replacement method from cuprous oxide, Cu_2O (Scheme 1). Importantly, this synthesis route is free of any capping agent or polymer, which enables a catalytically clean Pt surface. The presence of H^+ ions was found to be crucial for the reaction between $PtCl_4^{2-}$ and Cu_2O; otherwise this reaction cannot take place. Electrocatalytic properties of the as-prepared self-supported Pt NCs toward the ORR and MOR have been studied and compared with commercial Pt electrocatalyst materials.

Experimental section

Synthesis of Cu_2O nanocubes

Cu_2O nanocubes were prepared through a modified reductive solution chemistry route.[24] In a typical procedure, 0.50 g of poly(ethylene glycol) (PEG, M_w: 10 000) was first dissolved in 10 ml of $Cu(Ac)_2$ aqueous solution (0.1 mM). Then N_2 was purged into the reaction solution, and purging was maintained during the whole reaction process. Once PEG was completely dissolved, 50 μl of NaOH solution (6.0 M) was added dropwise. Upon addition, the solution immediately changed to blue color, indicating the formation of $Cu(OH)_2$ nanoparticles. After 10 min, 0.2 ml of AA solution (1 M) was added dropwise to the solution and it slowly turned to orange color. The products were collected by centrifugation after a reaction time of 30 min by repeatedly rinsing with DI water and ethanol in order to minimize the surface adsorbed PEG molecules.

Synthesis of Pt nanoclusters

5 mg of as-prepared Cu_2O nanocubes were ultrasonically re-dispersed in 5 ml of DI water. Then 5 ml of 10 mM K_2PtCl_4 aqueous solution were added to the Cu_2O suspension under magnetic stirring. At this stage, no reaction was observed as the solution remains orange (brown). To initialize the reaction, 0.1 ml of organic or inorganic acid was added to the reaction system. The solution immediately turned dark and then black, indicating the formation of Pt particles. The reaction was maintained for 1 h before the Pt nanoclusters were collected by centrifuging and rinsing with DI water and ethanol.

Characterization

Transmission electron microscopic (TEM) images were taken on a JEOL-3000F electron microscope. TEM samples were prepared by dropping the nanocrystal solution onto a carbon coated copper grid. The X-ray diffraction (XRD) patterns of the samples were conducted on a Rigaku/Max-3A X-ray diffractometer with Cu Kα radiation ($\lambda = 1.54178$ Å), the operation voltage and current were maintained at 40 kV and 40 mA, respectively.

Electrocatalysis

Electrochemical measurements were performed using a rotating disk electrode (RDE) in a conventional three-electrode cell with 0.5 M H_2SO_4 solution on a CHI Electrochemical Station (Model 750b) at room temperature. A graphite rod and an Ag/AgCl (3.0 M NaCl) electrode were used as the counter and reference electrodes, respectively. All potentials have been converted to the reversible hydrogen electrode (RHE) scale. In order to prepare catalyst ink, appropriate amounts of Pt nanoclusters, commercial Pt/C (20 wt%, E-TEK) and Pt black (Johnson Matthey) were ultrasonically dispersed in an alcoholic solution containing 5 wt% Nafion® ionomer for 1 h. The ink was then applied to the glassy-carbon disk of RDE with a geometric area of 0.254 cm^2. The Pt loading was controlled at 0.1 mg cm^{-2}. Steady-state polarization plots of the ORR were recorded in an O_2-saturated electrolyte. The potential step is 0.03 V holding for 30 s to eliminate the possible capacitance current. The electrochemical activities and ECSA were also characterized by cyclic voltammetry (CV). The working electrode was first cycled between 0.05 and 1.2 V for 50 cycles at 50 mV s^{-1} in a N_2-saturated 0.5 M H_2SO_4 solution to produce a clean electrode surface. Then the CV tests were performed at a scan rate of 10 mV s^{-1}. Accelerated durability tests were carried out in an O_2-saturated 0.5 M H_2SO_4 solution with the potential cycling between 0.6 and 1.1 V at a scan rate of 50 mV s^{-1}. The methanol oxidation reaction was carried out in 0.5 M H_2SO_4 solutions containing 1.0 M methanol.

Results and discussion

Cu_2O was synthesized through a modified reductive solution chemistry route.[24] Typically, Cu^{2+} ions were firstly precipitated into $Cu(OH)_2$ in blue color (eqn (1)), which was then reduced to Cu_2O by ascorbic acid (AA) following eqn (2) (AA* indicates the oxidized form of AA). Since Cu_2O can easily react with O_2, N_2 was purged into the reaction system during the synthesis. As shown in Fig. 1a, Cu_2O nanocubes with sizes of ~40 nm were obtained using our technique. The high-resolution (HR) TEM image inset in Fig. 1a reveals that these nanocubes are highly crystallized. Cu_2O nanocubes were then re-dispersed into water for the subsequent synthesis of Pt. Of note is that Cu_2O cannot directly react with $PtCl_4^{2-}$, as no reaction is observed even after a very long time (>8 h) when simply mixing Cu_2O with K_2PtCl_4 solution. No reaction occurred even by heating the mixture solution of Cu_2O and K_2PtCl_4 to 80 °C. However, a small amount of acid can "catalyze" the reaction, as the orange Cu_2O solution turns black immediately after the addition of acid, following eqn (3). This result agrees well with the electroless Pt deposition on Mn_3O_4 *via* a galvanic replacement process occurring between Mn_3O_4 and $PtCl_4^{2-}$ complexes.[20] Therefore, the presence of H^+

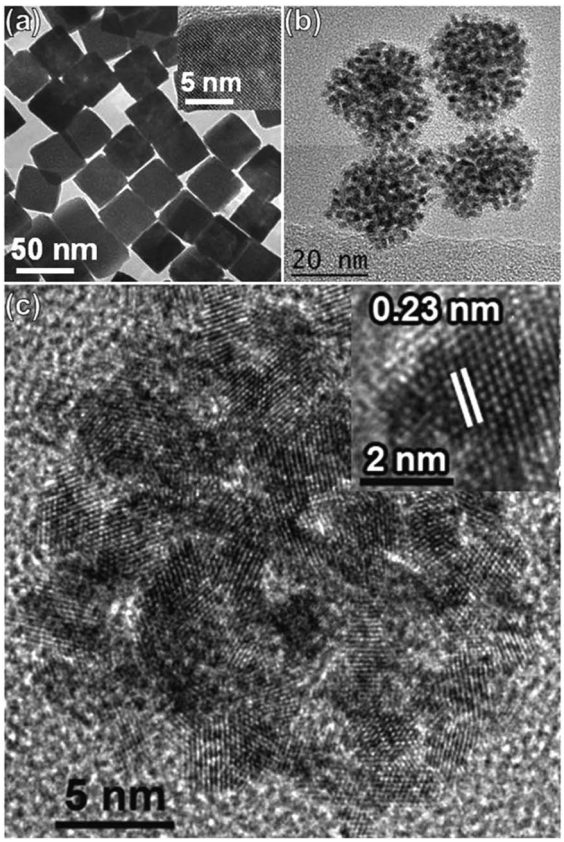

Fig. 1 TEM images of the as-prepared Cu_2O nanocubes (a), self-supported Pt nanoclusters prepared *via* galvanic replacement from Cu_2O (b), HR-TEM image of a single Pt assembly (c) and a single Pt nanoparticle (inset in (c)). The acid applied in the galvanic replacement is acetic acid.

ions is crucial for the production of Pt *via* the galvanic replacement from Cu_2O. Very recently, Liu *et al.*[21] reported an *in situ* growth of Au NPs on the surfaces of Cu_2O nanocubes, which involves the reduction of Au^{3+} ions by Cu_2O. However, the critical role of H^+ ions has not been realized since $HAuCl_4$ used as the Au precursor intrinsically contains H^+ ions. Here, we point out the critical role of H^+ ions in the reduction of Au^{3+} by Cu_2O, as we tried to reduce Au^{3+} ions by Cu_2O from $AuCl_3$ precursor, no Au NPs can be produced even after several hours.

$$Cu^{2+} + 2OH^- \rightarrow Cu(OH)_2 \quad (1)$$

$$Cu(OH)_2 + AA \rightarrow Cu_2O + AA^* \quad (2)$$

$$Cu_2O + 2H^+ + PtCl_4^{2-} \rightarrow Pt + 2Cu^{2+} + 4Cl^- + H_2O \quad (3)$$

After a reaction time of about 1 h, Cu_2O can be completely transformed into Pt without any solid copper residuals, as confirmed by an energy dispersive spectrometric (EDS) study (see Fig. S1†). Fig. 1b shows the Pt NCs prepared from the Cu_2O nanocubes, with an average size of about 20 nm. In the experiment, acetic acid was added to initialize the reaction. The individual Pt NPs that form the NCs are typically 2–3 nm in size, regardless of the size of Cu_2O nanocubes. The HR-TEM image in Fig. 1c clearly demonstrates that these 2–3 nm Pt NPs that form the NCs are interconnected to be self-supported and highly crystallized, with a similar porous structure as reported.[22,23] The HR-TEM image of a single Pt NP indicates that these NPs may prefer to grow along the (111) crystal planes (inset in Fig. 1c). The X-ray diffraction (XRD) pattern shows typical diffraction peaks that can be indexed to (111), (200), (220), (311), and (222) crystal planes of face centered cubic (fcc) Pt crystals, indicating the high degree of crystallinity of individual Pt NPs (see Fig. S1†). The broadening of the diffraction peaks can well match the size of the individual Pt NPs according to the Scherrer equation. As reported,[5] self-supported Pt nanostructures typically show better electrocatalytic performances than the carbon-supported Pt materials. Here, besides the formation of self-supported Pt NCs, another advantage of the developed galvanic replacement technique is that no capping agent or stabilizing agent is involved in the synthesis process to form the self-supported assembled structure. Moreover, Cu_2O becomes Cu^{2+} ions upon oxidation, and no Cu related residuals are present in the final Pt products. Therefore, the surfaces of these Pt NCs prepared using Cu_2O as sacrificing templates are catalytically clean, favorable for enhancing the electrocatalytic activity for the ORR and MOR.

Our previous studies demonstrated the acid-directed synthesis of Ag nanostructures and found that the acids can dramatically change the assembly manner of the Ag NPs, leading to various Ag nanostructures with complex morphologies.[25] Here, since H^+ ions are so crucial for the production of Pt, our immediate thought is that acids may impact the assembly manner and/or the morphology of the Pt NPs. Interestingly, we observe similar Pt NCs through the galvanic replacement from Cu_2O (see Fig. S2†) regardless of the acid we used, organic or inorganic. The individual Pt NPs that form the NCs are also 2–3 nm in size, and HR-TEM images confirm that the Pt NPs are highly crystallized (see Fig. S3†). We think it can be rationalized by the fact that galvanic replacement occurs from every surface of the Cu_2O NPs. The initial Cu_2O particles are comprised of numerous extremely small NPs somehow tightly bound with each other. Galvanic replacement simply exchanges the Cu_2O with Pt, and the produced Pt NPs tend to interconnect with others at the Cu_2O surface. When one Cu_2O particle is completely "eaten" by the $PtCl_4^{2-}$ ions, the produced Pt NPs spontaneously form NCs. This indicates that we do not have to choose a specific acid to induce the formation of such self-supported Pt NCs, but only the supply of H^+ ions to catalyze the reaction. Our work is in clear contrast with previous work that shows that the presence of macromolecular capping agent cetyltrimethyl ammonium bromide (CTAB) is crucial for the formation of an interconnected Pt structure.[5]

The electrocatalytic performance of the self-supported Pt NCs for the ORR has been evaluated, using the sample shown in Fig. 1b as a typical example. The ORR measurements were conducted in 0.5 M H_2SO_4 solution on a glassy carbon rotating disk electrode (RDE) at room temperature. We benchmarked the electrocatalytic properties of the Pt NCs toward ORR against both commercial Pt/C catalyst (20 wt%, E-TEK) and Pt black (Johnson Matthey). Prior to ORR tests, cyclic voltammetric (CV)

curves (Fig. 2a) of these three samples were recorded at room temperature in N_2-purged 0.5 M H_2SO_4 solutions at a scan rate of 10 mV s^{-1} for precisely evaluating the ECSA. The CV curves of as-prepared Pt NCs at different scan rates were also measured (Fig. S4†). The CV curves exhibited two featured potential regions associated with hydrogen adsorption/desorption processes between 0.05 and 0.37 V and the formation of Pt oxide beyond ~0.6 V. The ECSA was calculated by measuring the charge collected in the hydrogen adsorption/desorption regions after double-layer correction, assuming a value of 210 mC cm^{-2} for the adsorption of a hydrogen monolayer on polycrystalline Pt.[26] The measured specific ECSA (the ECSA per unit weight of metal) of the Pt NCs is 34.4 m^2 g_{metal}^{-1}, which is ~50% of the Pt/C catalyst (69.1 m^2 g_{metal}^{-1}) (Fig. 2c). The lower ECSA for the Pt NC catalyst is most likely due to the larger size arising from the interconnected structure as compared with that of Pt NPs (~3.2 nm, see Fig. S5†) in the commercial Pt/C catalyst. However, the specific ECSA of the Pt NCs is significantly larger than that measured with Pt black (18.6 m^2 g_{metal}^{-1}), presumably due to the unique assembled structure and highly porous structure as reflected by TEM images.

Fig. 2b shows the ORR polarization plots of the three catalysts, with a mixed kinetic-diffusion control region between 0.7 and 1.0 V. Mass transport limiting currents are observed for all three samples below 0.6 V, attesting sufficient active sites on the catalyst surface. In particular, the half-wave potentials ($E_{1/2}$) of the Pt NCs, Pt/C and Pt black are 0.868, 0.850, and 0.817 V, respectively, indicating that the activity of the Pt NCs is superior to those of both commercial Pt catalysts. More importantly, the observed $E_{1/2}$ on Pt NCs is also higher than that of the recently reported Pt nanotubes (0.84 V),[27] Pt nanocubes (0.71 V),[28] Pt nanowire membranes (0.83 V),[29] and interconnected Pt nanowires (0.84 V).[5] This much improved ORR activity is most likely due to the catalytically clean Pt NCs, free of "chemical contamination" induced by the capping agents and/or polymer surfactants, which are typically employed to stabilize the above Pt nanomaterials. Using kinetic current densities (j_k), mass activity (Pt utilization) and specific activity (intrinsic activity of Pt) are calculated by normalizing the Pt loading and ECSA of the catalyst, respectively. The kinetic current is calculated from the ORR polarization curve according to the Koutecky–Levich equation:

$$j_k = j \times j_d/(j_d - j) \quad (4)$$

where j_d is diffusion-limiting current density. As exhibited in Fig. 2d, Pt NCs have a mass activity of 42 A g_{metal}^{-1} at 0.85 V, which is 1.8 and 3.5 times greater than that of the Pt/C (23 A g_{metal}^{-1}) and Pt black (12 A g_{metal}^{-1}), respectively. Importantly, the specific activity measured with Pt NCs

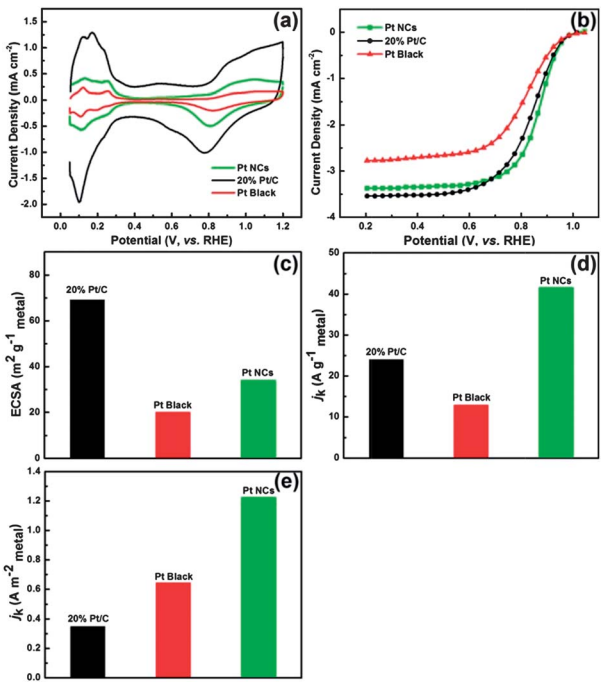

Fig. 2 Comparison of electrocatalytic properties between the commercial Pt/C (20 wt%), Pt black and as-synthesized Pt NCs; (a) CV curves obtained at room temperature in a N_2-saturated 0.5 M H_2SO_4 solutions at a scanning speed of 10 mV s^{-1}. (b) ORR steady-state RDE polarization curves in an O_2-saturated 0.5 M H_2SO_4 solution at room temperature with a rotating speed of 900 rpm. (c) Specific ECSAs for three catalysts. (d) Mass-transport corrected mass activity and (e) specific activity for three catalysts at 0.85 V.

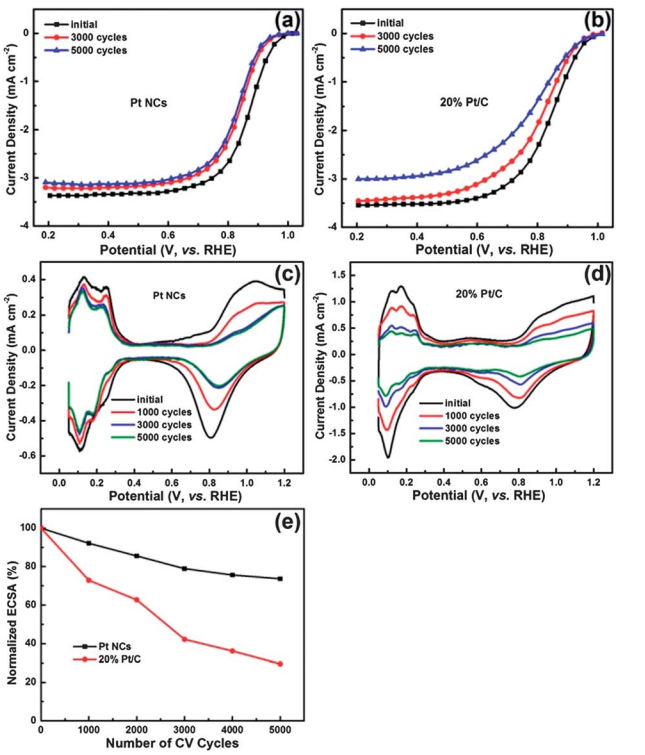

Fig. 3 Comparison of the ORR and electrochemical durability of commercial Pt/C (20 wt%) and Pt NCs. ORR steady-state RDE polarization curves recorded with a rotating speed of 900 rpm and CV curves obtained in N_2-saturated 0.5 M H_2SO_4 solutions at a scanning speed of 10 mV s^{-1} for Pt NCs (a and c) and Pt/C (b and d) after different numbers of cycles in an O_2-saturated 0.5 M H_2SO_4 solution at room temperature with the cyclic potential sweeping between 0.6 and 1.1 V at a scan rate of 50 mV s^{-1}. (e) Loss of ECSA of Pt NCs and Pt/C dependent on the number of CV cycles.

(1.22 A m_{metal}^{-2}) at 0.85 V is significantly higher than those of Pt/C (0.35 A m_{metal}^{-2}) and Pt black (0.63 A m_{metal}^{-2}) (Fig. 2e). In addition, the ORR kinetic current of the Pt NCs from Tafel plots (see Fig. S6†) is also higher than those of Pt/C and Pt black over the kinetically controlled potential range. The Tafel slope (b) calculated for the Pt NCs agrees well with those obtained on the Pt/C and Pt black, with −58 mV per decade at low potentials and −119 mV per decade at high potentials, respectively, suggesting identical ORR rate-determining steps (RDS) for all the three Pt catalysts.[30] Besides the benefits of a catalytically "clean" surface, the enhanced ORR activity of the Pt NCs relative to Pt/C and Pt black might be attributed to the preferential exposure of (111) crystal facets in the Pt NCs as well as the high surface area and more open structure. Besides the ORR activity, Pt NCs were also evaluated as electrocatalysts toward MOR, which is a kinetically sluggish reaction in direct methanol fuel cells (DMFCs). As shown in Fig. S7,† Pt NCs have improved MOR performance in the kinetic region, greater durability as well as a much higher peak current density relative to the commercial Pt/C catalyst.

The long-term durability of the electrocatalysts in fuel cell operation remains one of the main bottlenecks to be resolved as it greatly limits the widespread applications of fuel cells. In order to evaluate the electrochemical stability of the Pt NCs, accelerated durability tests (ADT) of the catalysts were conducted by cycling the potential between 0.6 and 1.1 V in an O_2-saturated 0.5 M H_2SO_4 solution at room temperature, which is close to the typical potential range at fuel cell cathodes.[3] After 5000 cycles, Pt NCs show ~30 mV loss of half-wave potential accompanying with a slight decrease in the diffusion-limited current (Fig. 3a). While, the Pt/C catalyst suffers from a more significant drop in the half-wave potential (~60 mV) and a noticeable decrease in the diffusion-limited current (Fig. 3b). Fig. 3c and d show the CV curves of the Pt NCs and Pt/C catalysts as a function of cycle numbers. In the case of commercial Pt/C, current densities of the peaks in the hydrogen adsorption/desorption region decrease substantially upon the increase of the cycle number. In addition, its capacitance current is reduced by ~40% after 5000 cycles, suggesting the occurrence of carbon corrosion. In contrast, the Pt NC catalyst (Fig. 3c) bears only a slight drop in the current densities of the peaks in the hydrogen region after 5000 cycles. In addition, the current decreases in the oxygen region (E > 0.6 V) after voltammetric cycling were observed with both catalysts and the current decrease measured with Pt/C was more significant than that on Pt NCs. This indicates that the formation of Pt oxides on the catalyst surface is remarkably hampered with both catalysts, most likely due to the particle agglomeration during the cycling test. Another reason that might account for the incapability to form Pt oxides on the catalyst surface is the reconstruction of the atomic surface structure over cycling tests, which results in a more densely packed surface structure.[31] The loss of ECSA of two catalysts over cycling tests is compared in Fig. 3e. After 5000 cycles, the Pt NCs lost only 26% of the initial ECSA, while a 71% drop of initial ECSA was detected for the Pt/C catalyst. In order to identify the possible reasons for the loss of ECSAs, the Pt NCs and Pt/C catalysts after the potential cycling tests were subjected to TEM characterization. Compared with the initial TEM image (see Fig. S5†), particle agglomeration and a broader size distribution are clearly observed for the Pt/C catalyst after 5000 cycles (see Fig. S8†), confirming that the major cause for the ECSA loss of Pt/C is due to the migration, agglomeration and Ostwald ripening concurrent with carbon corrosion.[27] In contrast to the Pt/C, only a slight morphological change of Pt NCs is observed after cycling tests. Interconnected assembly structure in Pt NCs is maintained with very minor size growth (see Fig. S9†). This should account for the small drop in ECSA of Pt NCs. The Pt NC catalyst is apparently free of Ostwald ripening, aggregation, and carbon corrosion, which thus can guarantee the remarkably high stability. As a result, the Pt NCs reveal superior initial ORR activity and much enhanced durability when compared with the commercial Pt catalysts, most likely due to their contamination-free and catalytically clean surface along with the unique self-supported interconnected and porous structure.[22,23,31]

Conclusions

In summary, self-supported Pt NCs comprised of interconnected 2–3 nm Pt NPs have been prepared *via* a novel galvanic replacement route from Cu_2O. Our results show that supply of H^+ ions is crucial for initializing the reaction, while no specific acid has to be chosen for the production of such Pt NCs. This synthesis procedure eliminates the use of any polymer capping agents and enables a catalytically clean Pt surface. The electrocatalytic performances of the Pt NCs for oxygen reduction and methanol oxidation reactions are far superior to commercial Pt materials, with higher electrochemical activity and greater long-term durability.

Acknowledgements

PX thanks support from the China Postdoctor Fund, NSFC (no. 21203045, 21101041, 21003029, 21071037, 91122002), Fundamental Research Funds for the Central Universities (no. HIT.NSRIF. 2010065 and 2011017, and HIT.BRETIII. 201223), and Director's Postdoctoral Fellow from LANL. HLW acknowledges the financial support from the Laboratory Directed Research and Development (LDRD) fund under the auspices of DOE. This work is partially supported by Basic Energy Science (BES), Biomaterials program, Materials Sciences and Engineering Division.

Notes and references

1 H. Lee, S. E. Habas, S. Kweskin, D. Butcher, G. A. Somorjai and P. D. Yang, *Angew. Chem., Int. Ed.*, 2006, **45**, 7824–7828.
2 N. Tian, Z. Y. Zhou, S. G. Sun, Y. Ding and Z. L. Wang, *Science*, 2007, **316**, 732–735.
3 B. Lim, M. J. Jiang, P. H. C. Camargo, E. C. Cho, J. Tao, X. M. Lu, Y. M. Zhu and Y. N. Xia, *Science*, 2009, **324**, 1302–1305.
4 L. Cademartiri and G. A. Ozin, *Adv. Mater.*, 2009, **21**, 1013–1020.
5 B. Y. Xia, W. T. Ng, H. Bin Wu, X. Wang and X. W. Lou, *Angew. Chem., Int. Ed.*, 2012, **51**, 7213–7216.

6 N. M. Markovic and P. N. Ross, *Surf. Sci. Rep.*, 2002, **45**, 121–229.
7 J. Yin, J. H. Wang, M. R. Li, C. Z. Jin and T. Zhang, *Chem. Mater.*, 2012, **24**, 2645–2654.
8 T. S. Ahmadi, Z. L. Wang, T. C. Green, A. Henglein and M. A. ElSayed, *Science*, 1996, **272**, 1924–1926.
9 Y. T. Yu and B. Q. Xu, *Appl. Organomet. Chem.*, 2007, **21**, 209.
10 H. Song, F. Kim, S. Connor, G. A. Somorjai and P. D. Yang, *J. Phys. Chem. B*, 2005, **109**, 188–193.
11 C. Wang, H. Daimon, Y. Lee, J. Kim and S. Sun, *J. Am. Chem. Soc.*, 2007, **129**, 6974–6975.
12 L. Hu, X. Q. Cao, L. Chen, J. W. Zheng, J. M. Lu, X. H. Sun and H. W. Gu, *Chem. Commun.*, 2012, **48**, 3445–3447.
13 S. H. Sun, F. Jaouen and J. P. Dodelet, *Adv. Mater.*, 2008, **20**, 3900–3904.
14 E. P. Lee, Z. M. Peng, W. Chen, S. W. Chen, H. Yang and Y. N. Xia, *ACS Nano*, 2008, **2**, 2167–2173.
15 S. Q. Ci, J. P. Zou, G. S. Zeng, S. L. Luo and Z. H. Wen, *J. Mater. Chem.*, 2012, **22**, 16732–16737.
16 A. Takai, Y. Yamauchi and K. Kuroda, *Chem. Commun.*, 2008, 4171–4173.
17 M. Sanles-Sobrido, M. A. Correa-Duarte, S. Carregal-Romero, B. Rodriguez-Gonzalez, R. A. Alvarez-Puebla, P. Herves and L. M. Liz-Marzan, *Chem. Mater.*, 2009, **21**, 1531–1535.
18 I. J. Hsu, D. V. Esposito, E. G. Mahoney, A. Black and J. G. G. Chen, *J. Power Sources*, 2011, **196**, 8307–8312.
19 D. G. Li, C. Wang, D. Tripkovic, S. H. Sun, N. M. Markovic and V. R. Stamenkovic, *ACS Catal.*, 2012, **2**, 1358–1362.
20 K. W. Kim, S. M. Kim, S. Choi, J. Kim and I. S. Lee, *ACS Nano*, 2012, **6**, 5122–5129.
21 X. W. Liu, F. Y. Wang, F. Zhen and J. R. Huang, *RSC Adv.*, 2012, **2**, 7647–7651.
22 R. Pasricha, T. Bala, A. V. Biradar, S. Umbarkar and M. Sastry, *Small*, 2009, **5**, 1467–1473.
23 X. W. Teng, X. Y. Liang, S. Maksimuk and H. Yang, *Small*, 2006, **2**, 249–253.
24 L. F. Gou and C. J. Murphy, *Nano Lett.*, 2003, **3**, 231–234.
25 B. Zhang, P. Xu, X. M. Xie, H. Wei, Z. P. Li, N. H. Mack, X. J. Han, H. X. Xu and H. L. Wang, *J. Mater. Chem.*, 2011, **21**, 2495–2501.
26 S. Trasatti and O. A. Petrii, *Pure Appl. Chem.*, 1991, **63**, 711–734.
27 Z. W. Chen, M. Waje, W. Z. Li and Y. S. Yan, *Angew. Chem., Int. Ed.*, 2007, **46**, 4060–4063.
28 C. Wang, H. Daimon, T. Onodera, T. Koda and S. H. Sun, *Angew. Chem., Int. Ed.*, 2008, **47**, 3588–3591.
29 H. W. Liang, X. A. Cao, F. Zhou, C. H. Cui, W. J. Zhang and S. H. Yu, *Adv. Mater.*, 2011, **23**, 1467–1471.
30 C. Coutanceau, M. J. Croissant, T. Napporn and C. Lamy, *Electrochim. Acta*, 2000, **46**, 579–588.
31 S. Y. Wang, S. P. Jiang, T. J. White, J. Guo and X. Wang, *J. Phys. Chem. C*, 2009, **113**, 18935–18945.

